Solid Freeform Fabrication 2016: Proceedings of the 27th Annual International Solid Freeform Fabrication Symposium – An Additive Manufacturing Conference
Reviewed Paper

Simulation of Cooling Rate Effects on Ti-48Al-2Cr-2Nb Crack Formation in Direct Laser Deposition

Lei Yan[1], Wei Li[1], Xueyang Chen[1], Yunlu Zhang[1], Joe Newkirk[2], Frank Liou[1], David Dietrich[3]
[1]Department of Mechanical and Aerospace Engineering
[2]Department of Materials Science and Engineering
Missouri University of Science and Technology, Rolla, MO
[3]The Boeing Company, St. Louis, MO

Abstract

Transient temperature history is vital in direct laser deposition (DLD) because it reveals the cooling rate at specific temperatures, which directly relates to phase transformation and types of microstructure formed in deposit. FEA simulation was employed to study the transient temperature history and cooling rate at different experimental setups in Ti-48Al-2Cr-2Nb DLD process. In this paper, an innovative model was described, which combines a moving Gaussian distribution heat source and element birth and death technology in ANSYS, help to analysis cooling rate control method and guide crack-free deposits build process.

1. Introduction

Dual phase gamma titanium aluminides (γ-TiAl) has been seen as a promising candidate material in high temperature aerospace and automotive gas turbine engines to replace Ni-based superalloys for its high specific strength, high stiffness, good corrosion resistance, high creep resistance between 600 ~ 750 ºC, and oxidation resistance (Kothari et al. 2011; Guoqing et al. 2011). Ingot metallurgy (IM) process followed by hot isostatic pressing (HIP) are commonly accepted by industry for raw γ-TiAl material preparation and porosities elimination before high temperature thermos-mechanical processing (Sun et al. 2012). High production cost become a key drawback of γ-TiAl to be widely used compared to Ni-based superalloys (Kothari, Radhakrishnan, and Wereley 2011). Also, its brittleness and low fracture toughness makes γ-TiAl difficult to manufacture with conventional methods. Direct laser deposition (DLD) is a viable and promising technology that has revolutionized manufacturing complex and hard-manufactured material components (Yan, et al. 2015). The complexity of thermodynamics in deposition process is critical to final part's mechanical properties. In this paper, DLD was utilized to build multilayer thin-wall structure with commercially available γ-TiAl powder Ti-48AL-2Cr-2Nb. A three-dimensional nonlinear finite element model of multiple layers thin-wall structure was presented with element birth and death procedures in ANSYS. The numerical simulation results were used to understand the formation of cracks based on phase transformation and provide guides to build crack-free deposit.

2. Finite element modeling for DLD process

A three-dimensional finite element model was developed to simulate the DLD process using ANSYS APDL. Element birth and death procedures were used to simulate material added process. This model could be used to predict temperature history, cooling rate, and residual stress during and after deposition process till cooling to room temperature.

The final part was built with CP Ti substrate and γ-TiAl thin-wall structured deposit on it. The geometry and finite element mesh used in the model is shown in Fig. 1. The substrate has a 50mm long (L_1), 12.5mm wide (L_2), and 6.25mm thick (L_3). The deposit with 50 layers was built on the substrate surface, each layer with a length of 20mm, a thickness of 0.1mm, and a width of 1.8mm, which equals to the laser beam diameter. Laser transvers speed is 600 mm/min and moves from left to right in odd number layers and from right to left in even number layers.

The finite element model was divided into different parts before meshing based on how the sensitivity in different parts relate to the simulation results. Based on this strategy, a dense mesh was used in the deposit locations and the locations that contact the substrate. Other parts were meshed with a coarse mesh and the meshed model has 53716 nodes and 44960 elements totally. This mesh strategy guaranteed the simulation accuracy and with a reasonable convergence speed.

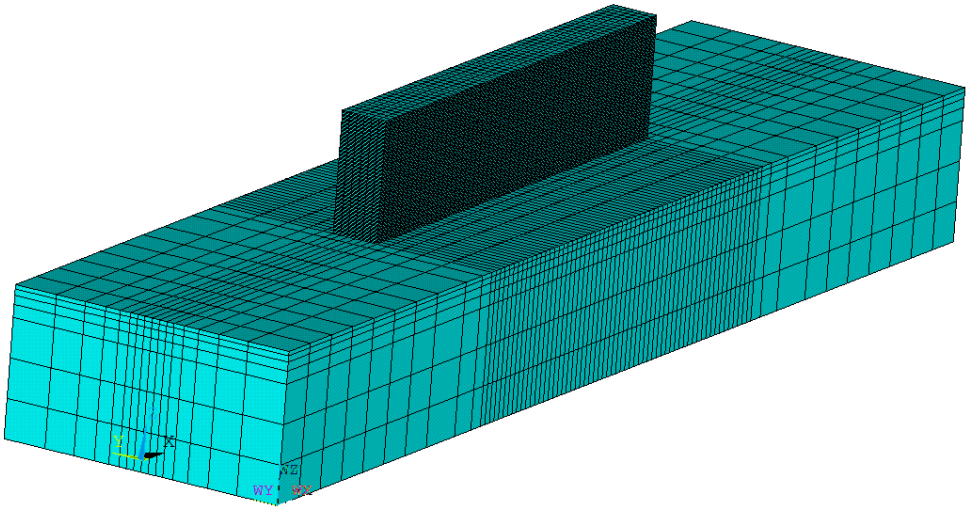

Fig. 1 Finite element mesh to simulate a 50-layer DLD process

2.1 Mathematical model

Using FEA to simulate the temperature distribution during DLD process is the effort to numerically solve the three dimensional heat diffusion equation (1):

$$\nabla \cdot k\nabla T + \dot{q} = \rho c_p \frac{\partial T}{\partial t} \qquad (1)$$

Where T is temperature, t is time, C_p is specific heat, ρ is density, k is thermal conductivity, ∇ is Hamilton operator which equals to $(\frac{\partial}{\partial x}, \frac{\partial}{\partial y}, \frac{\partial}{\partial z})$. In the DLD process there was no internal heat source so $\dot{q} = 0$. The density, thermal conductivity, and specific heat are all temperature-dependent parameters and the latent heat effects are modeled with the specific variation as shown in equation (2) (Toyserkani, et al. 2004).

$$c_p^*(T) = c_p(T) + \frac{L}{T_m - T_0} \qquad (2)$$

Where $c_p^*(T)$ is the modified specific heat, $c_p(T)$ is the original temperature-dependent specific heat, L is the latent heat of fusion, T_m is the melting temperature, and T_0 is the ambient temperature. Material temperature-dependent properties of Ti are as shown in Fig. 2 (Mills 2002) and γ-TiAl in Table 1 (Chen 2007).

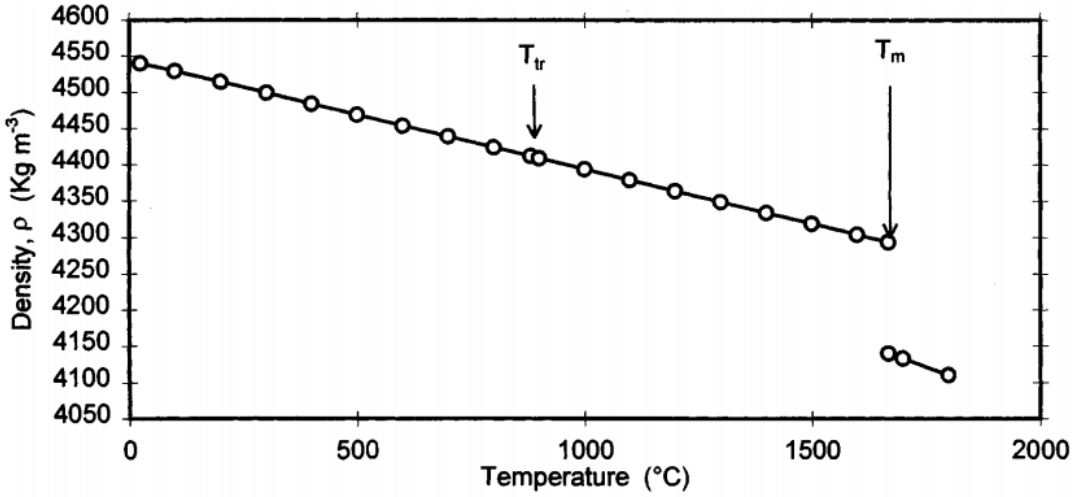

(a)

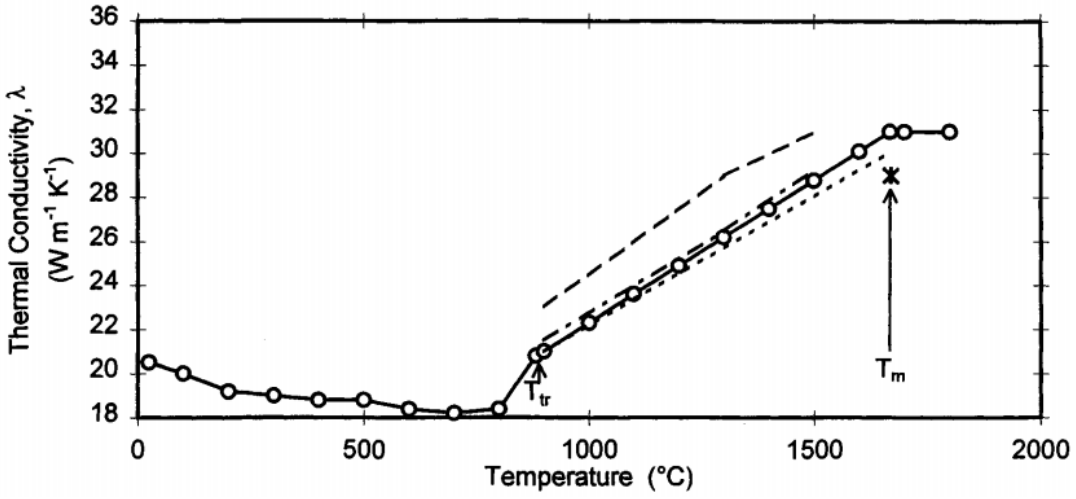

(b)

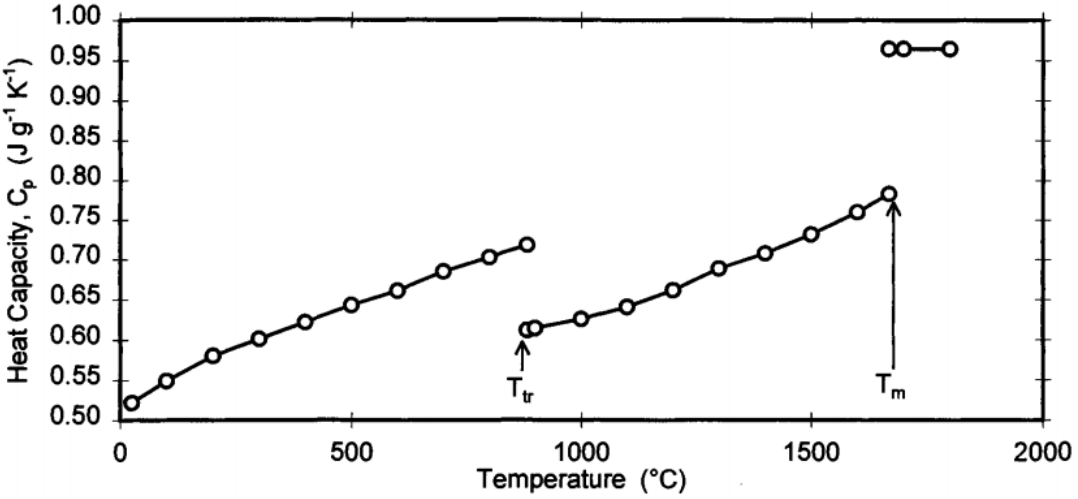

(c)

Fig. 2 Temperature-dependent properties used for CP Ti, (a) density, (b) thermal conductivity, (c) specific heat.

Table 1 Thermal physical parameters of TiAl at different temperatures

Temperature / ºC	25	150	300	450	600	900
Young's Modulus E / GPa	172	166.5	162	157.5	153	144
Yield Strength σ_s / MPa	359.9	373.7	358.9	336.7	329.3	259
Thermal Expansion $10^{-6}K^{-1}$	11	11.7	12.3	13.2	14	15
Thermal Conductivity $\lambda/$ $Wm^{-1}K^{-1}$	12	14	15	17.5	21	24
Specific Heat $c_p/JKg^{-1}K^{-1}$	400	430	465	500	520	600
Poisson's Ratio	0.22	0.22	0.22	0.22	0.22	0.22

2.2 The element birth and death method

The finite element model uses fixed mesh size for both substrate and deposit during simulation. To simulate the addition of material in DLD process a method call element birth and death in ANSYS was employed. The model was built with both death and birth elements initially. Element death means elements were given a status of deactivated by setting its stiffness to zero but the element technically still present. Birth is to restore element's stiffness and put it into calculation and a status of activated. Initially elements of substrate were given a status of activated but all the deposit elements were given a deactivated status, as the laser beam moves a group of elements would be selected and put into activated status at the beginning of each step, all those dynamic selection behaviors were defined with ANSYS APDL. The element birth and death method is demonstrated in Fig. 3.

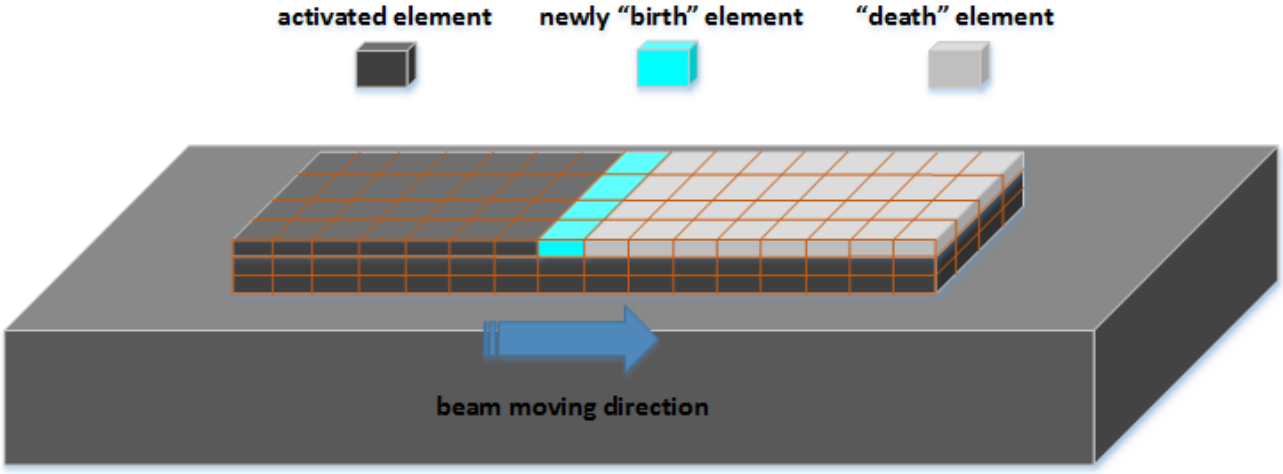

Fig. 3 Schematic of element birth and death method

2.3 Heat input, initial and boundary conditions

During DLD process, the laser beam moving along width center line back and forth. The moving laser beam was defined as Gaussian beam, with beam diameter D at the location of $\frac{1}{e^2}$ and expressed as equation (3):

$$I(x,y) = \frac{\alpha P}{\frac{1}{2}\pi\left(D/2\right)^2} e^{-2\left[(x-X)^2+\left(y-L_2/2\right)^2\right] \Big/ \left(D/2\right)^2} \quad (3)$$

Where α is power absorption coefficient and set to 0.4 for MST LAMP DLD system (Fan and Liou 2012), P is beam power (W), D is beam diameter and was set to 1.8 mm during DLD process, X is laser beam location along length direction and is defined by beam speed $V(t)$ (m/s), L and L_2 is dimension to determine beam starts point.
The initial condition (IC) of the numerical simulation domain was set to a uniform temperature field that equals to ambient temperature and was set to 300 K, which defined in equation (4).

$$T|_{t=0} = T_0 \quad 0 \le x \le L_1, 0 \le y \le L_2, 0 \le z \le L_3 \qquad (4)$$

The boundary conditions (BCs) for all other surfaces from both substrate and deposit at each step with laser energy input and heat loses from convection and radiation is defined as equation (5) (Wang et al. 2008):

$$k(\nabla T \cdot \vec{n})|_{\Omega} = h(T - T_a)|_{\Omega} + \varepsilon\sigma\left(T^4 - {T_e}^4\right)|_{\Omega} - Q_r|_{\Omega Laser} \qquad (5)$$

Where h is convective heat transfer coefficient, T_a is the ambient temperature, ε is emission coefficient of outer surfaces, σ is the Stefan-Boltzmann constant ($5.67 \times 10^{-8} W/m^2K^4$), T_e is the wall temperature of the sealed chamber and set equals to T_a, Q_r is the heat input from laser beam. As new elements changed from death to birth status the outer surfaces related to boundary conditions were updated.

3. Experimental setup and procedures

Thin-wall structured samples were fabricated with side nozzle DLD system, which includes an argon-purged chamber, 1 kW Nd-YAG fiber laser, powder feeder, and a 3-axis numerical control work table. Fig. 4 shows the experimental setup of the DLD system (Yan, et al. 2015).

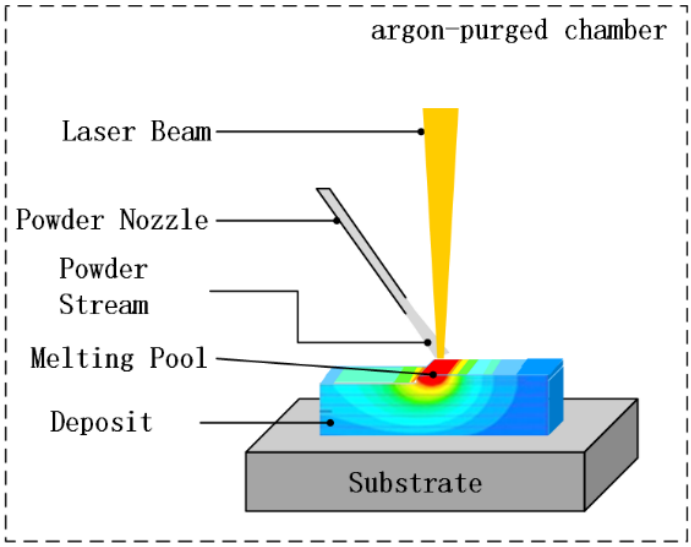

Fig. 4 Schematic of the DLD system

Two sets of experiment setup were used during deposition and the main difference between them was the substrate clamp method, one has the substrate contact with steel fixture directly and the other with insulating brick in between substrate and fixture. Fig. 5 shows the details of two experiment setups.

(a) *(b)*

Fig. 5 Two experiment setups used, (a) without insulating brick, (b) with insulating brick

In order to keep melt pool dimension similar within each layer, some cases were pre-studied and simulated with different laser transverse speed and laser power in order to obtain one optimized combination of laser energy density and laser transverse speed, where energy density is defined as $p = E/l$, E is input energy and l is the distance laser beam moves within the time those energy applied. In this study, laser transvers speed was set to 600 mm/min. Fig. 6 (a) shows how energy density changes with layer number. The very first layer with a much higher value due to more energy needed to generate melt pool. Fig. 6 (b) shows details of how the energy density changes from the second layer to the fiftieth, it could be found that the curve becomes less sloped as more layers are deposited. That is due to the slow heat transfer ability of thin-wall structure that leads to heat accumulating in the deposit as subsequent layers are added, which cause less input energy needed to maintain a similar melt pool size for the following layers. Also, idle time at two ends of each layer, with reduced laser energy density, was applied in order to increase thin-wall structure shape quality, which helped to eliminate material loss caused by moving stage direction change and built more rectangular structure.

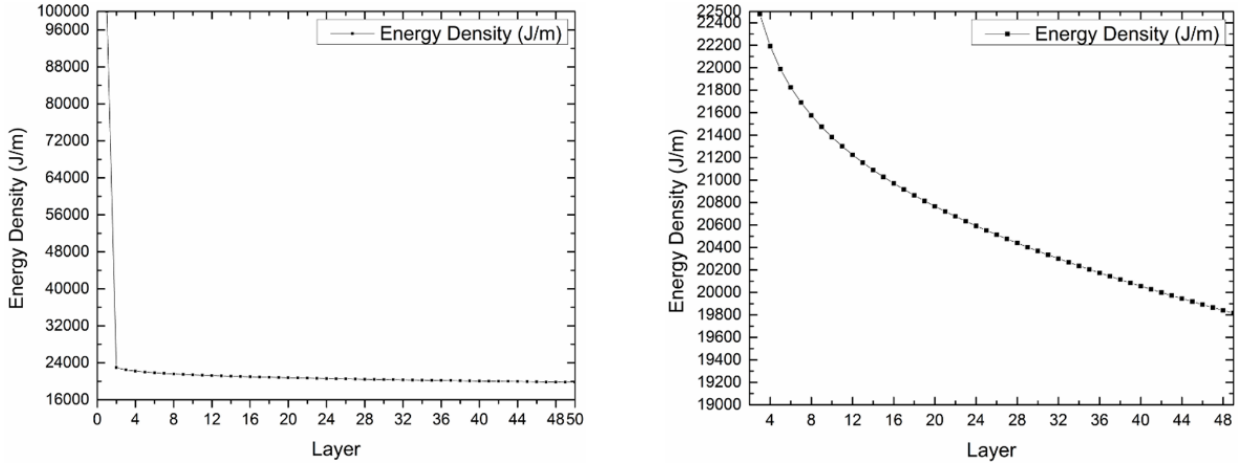

(a) *(b)*

Fig. 6 Energy density strategy, (a) energy density for the whole DLD process, (b) zoom out for layer 2 to 50.

The substrate used was commercially pure grade 2 titanium plate, sold by Titanium Processing Center. The powder used during deposition is commercially available gas atomized Ti-48Al-2Cr-2Nb powder from ATI Powder Metals LLC. Powder characters are listed in Table 2 and Table 3.

Table 2 Chemical Analysis of Ti-48Al-2Cr-2Nb powder (wt.%)

Ti	Al	Cr	Nb	Fe	Si	C	O
Bal.	34.4	2.38	4.75	0.04	0.016	0.014	0.128

Table 3 Powder Sieve Analysis ASTM B214 (% Under)

US Standard Mesh	-100	-140	-200	-230	-270	Apparent Density
Opening in Microns	150	106	75	63	53	(ASTM B212) (g/cc)
	99.9	66.2	25.5	14.7	4.0	2.20

4. Results and discussions

Deposition experiment on two sets of experiment setup were performed and FEA simulation was employed and help to understand the transient temperature history and cooling rate under different experiment setup.

Fig. 7 (a) and (b) shows 50-layer deposit built under different experiment setup, the first one, which had vertical cracks, was built without insulating bricks and idle time at the two ends, the second, which was a crack-free final part, was built with insulating bricks and idle time at the two ends. Both deposits were well bonded with substrate as 1kw laser power was used for the first layer. Those two deposits were cross sectioned with EDM cut, mounted, and polished according to standard metallographic preparation of Ti-48Al. The samples were then etched by Kroll's reagent consisting of 92 ml distilled H_2O, 6 ml HNO_3, and 2 ml HF to reveal different microstructures for further analysis. Fig. 7 (c) reveals micro-cracks distributed across the whole area of Fig. 7 (a). Fig. 7 (d) shows the microstructure of crack-free deposit showed in Fig. 7 (b) and lamellae was the main microstructure.

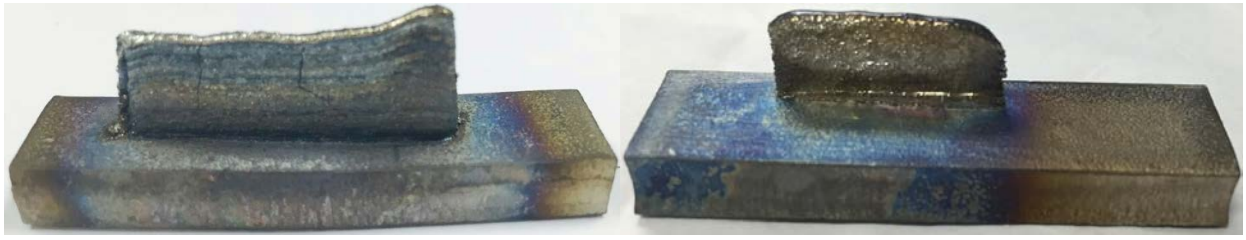

(a) *(b)*

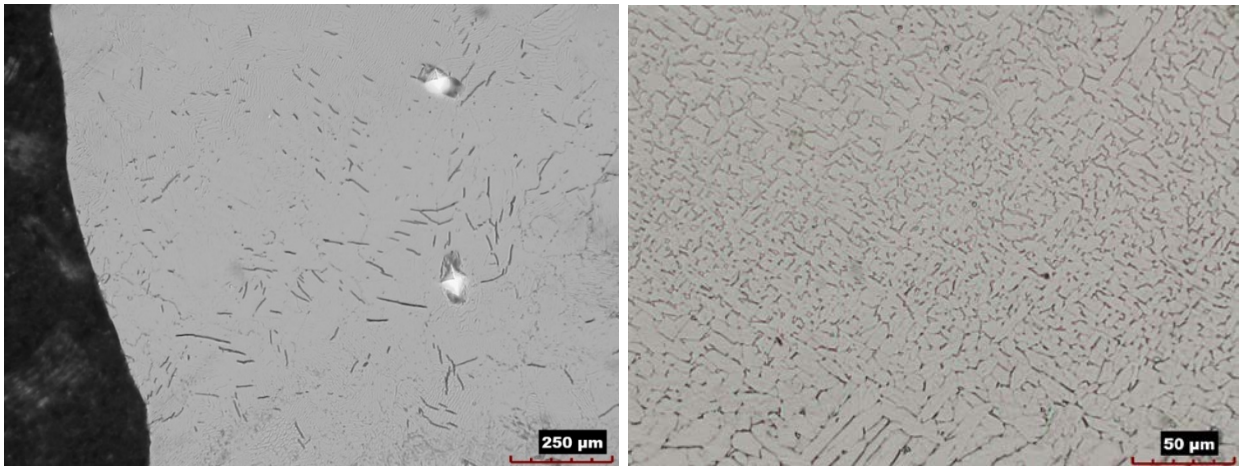

(c) *(d)*

Fig. 7 Deposit and microstructure, (a) cracked deposit, (b) crack-free deposit, (c) micro-crack in Fig.7 (a), (d) microstructure of crack-free deposit in Fig.7 (b).

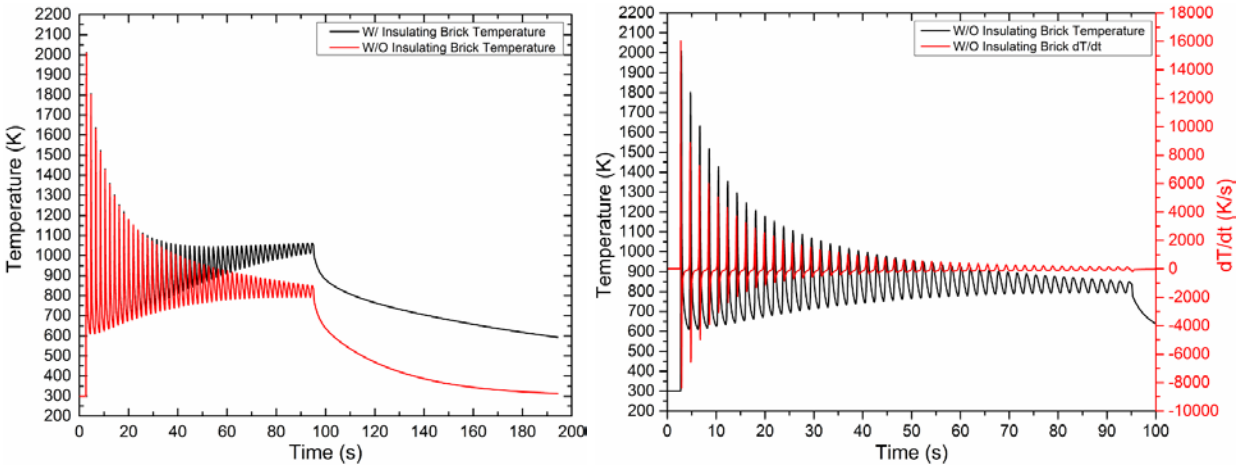

(a) *(b)*

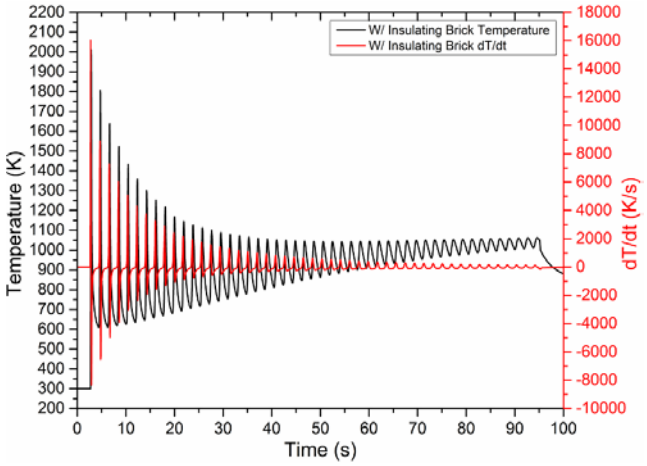

(c)

Fig. 8 FEA simulation results of two experiment setup, (a) temperature cycle for mid-point of layer 2,(b)temperature cycle and cooling rate without insulating brick,(c) temperature cycle and cooling rate with insulating brick

Fig. 8 shows the FEA simulation results of temperature history for the middle point of layer two. Fig. 8 (a) shows the thermal cycle with different experiment setup. Each peak indicates the laser beam passes over the pre-defined point, from initial layer to subsequent layers. The initial peak value is approximately 2025 K for both experiment setup and the following ten peak values are close to each other regardless of the presence of the insulating brick. After about twenty layers, the one with insulating brick has almost unchanged peak temperature around 1050 K but the other one has peak temperature decrease layer by layer, which means the insulating brick is in a sealed chamber played a furnace role and restrained heat loss via conduction to clamp fixture.

Fig. 8 (b) and (c) shows temperature cycle and temperature change rates for both experiment setups. The positive peaks indicate heating rate which means the second layer's mid-point is heated up when the laser beam passes over, and the negative peaks shows a cooling rate which shows the second layer's mid-point cools down as laser beam passes by from the initial layer to subsequent layers until deposition is completed. The initial maximum cooling rate for both experiment setups are about 8340 K/s. After that, the maximum cooling rates decrease as following layers were deposited and lead to the changes of temperature gradient become slow. After about forty layers were deposited, deposition with an insulating brick applied has maximum cooling rate of approximately 50 K/s and without the insulating brick of about 100 K/s. After deposition is completed, both experimental setups' maximum cooling rate decreased to less than 10 K/s after 100 seconds cooling. Other layers during deposition experienced similar thermal cycle and temperate change rates as the second layer, the difference is the maximum cooling rate for each layer's pre-defined point decreases as subsequent layers were deposited and it's due to the integrated heat of substrate and previous layers (Wang et al. 2008).

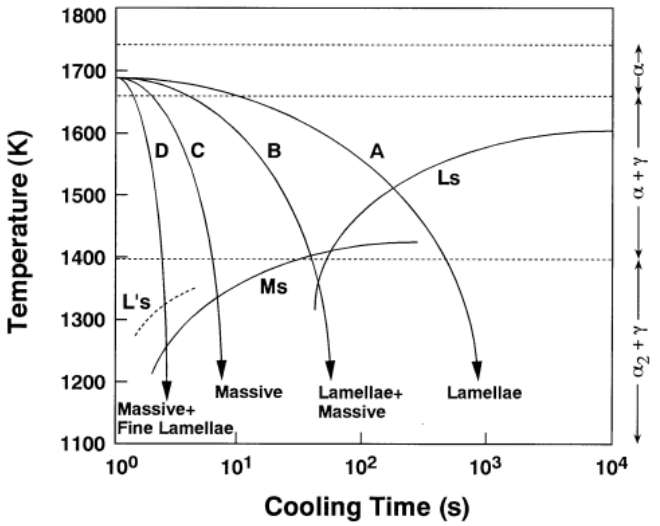

Fig. 9 Schematic CCT diagram for Ti-48Al: Ls and Ms represent lamellar and massive start lines.

Fig. 9 shows the schematic CCT diagram for Ti-48Al and curves A, B, C, and D represents cooling rate 1 K/s, 10 K/s, 100 K/s, and 1000 K/s separately (Matthias 2003; Kumagai and Nakamura 1998). It's revealed that cooling rate above 800 K/s the phase transformation would follow $L \rightarrow \beta \rightarrow \alpha + \beta \rightarrow \alpha + B_2 \rightarrow \alpha_2 + B_2$ and leads to phase transformation of $\alpha \rightarrow \gamma_m + (\alpha_2 + \gamma)_L$ being restrained, where B_2 and γ_m represents untransformed β and massive γ separately (Chen 2007). The ordering change of α→α_2 happens and α_2 phase will keep until

ambient temperature (Chaturvedi et al. 2001). The retained α and brittle α_2 phases are the main reason for cracking during cooling. Based on analysis of simulation results of the crack free deposit, maximum cooling rates around temperature 1670 K and 1400 K were about 5000 K/s and 2500 K/s, respectively, which means combination of massive γ and fine lamellae α_2 was formed. The critical cooling rate for high-temperature α phase to fully decompose is 250 K/s (Chaturvedi et al. 2001) and this maximum cooling rate is achieved when laser beam moves to layer twenty-five, without the insulating brick (peak temperature is about 950 K), and to twenty-two, with the insulating brick (peak temperature is about 1050 K), which can be seen from Fig. 8 (b) and (c). The insulating brick helps to keep the deposit stays at a higher temperature around 1050 K for a longer time than the experiment without the insulating brick applied, which benefits the phase transformation of $\alpha(\alpha_2) \rightarrow \gamma$ and results in the increase of γ phase volume fraction in the final part. The volume fraction increase of γ phase would increase the ductility of deposit and reduce cracks (Chen 2007). After deposition was completed, the deposit was cooled in a chamber and the cooling rate was less than 10 K/s and lamellae microstructure would be formed finally as Fig. 7 (d) shows. From above analysis it could be concluded that keeping the deposit at a high temperature around 1050 K for some time would result full decomposition of phase α and formation of phase γ which would lead to final part ductility increase and avoid cold cracks.

5. Conclusions

The results of this study can be summarized in the following points:

1) Cold cracks could be prevented during direct laser deposition of Ti-48Al-2Cr-2Nb by using an insulating brick to decrease the cooling rate.
2) Insulating brick helps to keep deposit at high temperature for a longer time that results in the decomposition of $\alpha(\alpha_2)$ phase and the formation of γ phase, which would result in a ductility increase in the final deposit.
3) The main microstructure in the crack-free deposit is lamellae and results from cooling rate less than 10 K/s.
4) FEA simulation provides a reliable way to analyze phase transformation and guidelines for crack-free deposit build.

Acknowledgements

This project was supported by The Boeing Company through the Center for Aerospace Manufacturing Technologies (CAMT), National Science Foundation Grant # CMMI-1547042, and the Intelligent Systems Center (ISC) at Missouri S&T. Their financial support is greatly appreciated.

References

Chaturvedi, M. C., Q. Xu, and N. L. Richards. 2001. “Development of Crack-Free Welds in a TiAl-Based Alloy.” *Journal of Materials Processing Technology* 118 (1-3): 74–78.

Chen, Guoqing. 2007. “Investigation on the Microstructure of TiAl Intermetallic Compound Electron Beam Welded Joints and the Crack Control Technology.”

Fan, Zhiqiang, and Frank Liou. 2012. “Numerical Modeling of the Additive Manufacturing (AM) Processes of Titanium Alloy.” *Titanium Alloys - Towards Achieving Enhanced Properties for Diversified Applications*, 3–28.

Guoqing, Chen, Zhang Binggang, Liu Wei, and Feng Jicai. 2011. “Crack Formation and Control upon the Electron Beam Welding of TiAl-Based Alloys.” *Intermetallics* 19 (12). Elsevier

Ltd: 1857–63.
Kothari, Kunal, Ramachandran Radhakrishnan, and Norman M. Wereley. 2011. "Characterization of Rapidly Consolidated γ-TiAl." *Journal of Engineering Materials and Technology* 133 (2): 024501.
Kumagai, Tatsuo, and Morihiko Nakamura. 1998. "Microstructure Evolution through the A~~γ~~ Phase Transformation in a Ti-48 At. Pct Al Alloy." *Metallurgical and Materials Transactions A* 29 (January): 19–26.
Matthias, Charpentier. 2003. "Hétérogénéités Héritées de La Solidification et Formation Des Microstructures Dans L'alliage Ti-48Al-2Cr-2Nb: Contribution Au Développement Des Alliages Intermétalliques de Base γ-TiAl." *Journal of Chemical Information and Modeling* 53 (9): 1689–99.
Mills, Kenneth. 2002. *Recommended Values of Thermophysical Properties for Selected Commercial Alloys*.
Sun, Hong Fei, Xue Wen Li, Jie Feng, and Wen Bin Fang. 2012. "Characterization of TiAl-Based Alloy with High-Content Nb by Powder Metallurgy." *Transactions of Nonferrous Metals Society of China (English Edition)* 22 (SUPPL.2): 491–95.
Toyserkani, Ehsan, Amir Khajepour, and Steve Corbin. 2004. "3-D Finite Element Modeling of Laser Cladding by Powder Injection: Effects of Laser Pulse Shaping on the Process." *Optics and Lasers in Engineering* 41 (6): 849–67.
Wang, L., S. Felicelli, Y. Gooroochurn, P. T. Wang, and M. F. Horstemeyer. 2008. "Optimization of the LENS Process for Steady Molten Pool Size." *Materials Science and Engineering A* 474 (1-2): 148–56.
Yan, Lei; Chen, Xueyang; Li, Wei; Liou, Frank; Newkirk, Joe. 2015. "DIRECT LASER DEPOSITION OF Ti-6Al-4V FROM ELEMENTAL POWDER BLENDS."